Global total precipitable water variations and trends during 1958-2021

Nenghan Wan[1], Xiaomao Lin[1*], Roger A. Pielke Sr.[2], Xubin Zeng[3], and Amanda M. Nelson[4]

[1]Department of Agronomy, Kansas Climate Center, Kansas State University, Manhattan, KS.
5   [2]Cooperative Institute for Research in Environmental Sciences, University of Colorado, Boulder, CO.
[3]Climate Dynamics and Hydrometeorology Center at the University of Arizona, Tucson, AZ.
[4]National Center of Alluvial Aquifer Research, USDA-ARS Sustainable Water Management Research Unit, Stoneville, MS.

Correspondence to: Xiaomao Lin (xlin@ksu.edu)

Abstract. Global responses of the hydrological cycle to climate change have been widely studied but uncertainties still remain

10   regarding water vapor responses to lower tropospheric temperature ~~of temperature responses to lower tropospheric water vapor still remain~~. Here, we investigate the trends in global total precipitable water (TPW) and surface temperature from 1958 to 2021 using ~~improved~~ ERA5 and JRA-55 reanalysis datasets and further validate these trends by using radiosonde from 1979 to 2019, Atmospheric Infrared Sounder (AIRS), and Microwave Satellite (SSMI(S)) observations from 2003 to 2021. Our results indicate a global increase in total precipitable water (TPW) of ~~0.66~~~2 % per decade ~~according to ERA5 data~~ from 1993-

15   2021 ~~and 0.88% per decade in JRA-55 data~~. These variations in TPW reflect the interactions of global warming feedback mechanisms across different spatial scales. Our results also revealed a significant near-surface temperature (T_{2m}) warming trend ~0.15 K per decade during 1958-2021. Its consistent warming at a rate of ~0.21 K per decade after 1993 ~~at the rate of 0.14 K dec^{-1}~~ corresponds to ~~and~~ a strong water vapor response to temperature at a rate of 49.5 ~~6~~% K^{-1} globally, with land areas warming approximately twice as fast as the oceans. The relationship between TPW and T_{2m} ~~or surface skin temperature (T_s)~~

20   showed a variation around 6 - 8% K^{-1} in the 15-~~60~~55 ºN latitude band, aligning with theoretical estimates from the Clausius–Clapeyron equation.

1 Introduction

As the most critical greenhouse gas in the Earth's atmosphere, water vapor plays a key role in atmospheric processes from the microscale (including the formation of clouds and precipitation) to the global scale, and is related to the Earth's radiation

25   budget, hydrological cycle, and climate change (Held and Soden, 2006; Lacis et al., 2010; Ruckstuhl et al., 2007). The amount of water vapor is primarily controlled by the air temperature when the relative humidity (especially over the ocean) remains unchanged in the low troposphere. The total precipitable water (TPW), also known as the column-integrated amount of water vapor from the surface to the top of the atmosphere, increases by 6-7% with a 1 K increase in air temperature according to the Clausius-Clapeyron equation and thus enhances the strength of global warming with strong positive feedback due to the

30   greenhouse effect (Held and Soden, 2006, O'Gorman and Muller, 2010) particularly in upper troposphere whereas changes at

lower levels are strongly linked with precipitation patterns, influencing the frequency and intensity of extreme weather events (Trenberth, 1998; Trenberth et al., 2003). Therefore, evaluating the long-term trend of TPW change and its relationship with temperature is important for understanding the role of water vapor in climate change and the impact of water vapor feedback on global warming.

35

Because of the short residence time of water vapor in the atmosphere, studies in terms of long-term water vapor trends and their variability still face challenges. The two main categories of water vapor data include observations collected from various weather station networks and satellites, as well as reanalysis datasets integrated with simulations and observations. The former has difficulty in evaluating long-term trends due to discontinuities, insufficient spatial densities, and coverage (Dee et al.,

40 2011). For example, radiosonde observations have the issue of spurious discontinuities or changes in variability due to shifts in instruments and observational methods (Dee et al., 2011; Trenberth et al., 2005). However, multiple observations have been homogenized and thoroughly quality-checked in recent years. For example, the ground-based measurements of Global Navigation Satellite Systems (GNSS) integrated water vapor from 1994-2021 (Bock, 2022) and provided evidence of global moistening (Douville et al., 2022). The in-situ observations from the Radiosounding HARMonization (RHARM) dataset

45 (Madonna et al., 2022) enhance the spatial consistency of estimated trends and align more closely with a contemporary atmospheric reanalysis. In addition, the homogenized temperature data presented by Zhou et al. (2021) exhibited spatially consistent trends and temporally stable variations, and didn't show the erroneous tropospheric cooling observed in various reanalyses including ERA5 and raw datasets, across North China and Mongolia. This accuracy of temperature can help in increasing the confidence in tropospheric temperature and water vapor, as well as in enhancing the quality of atmospheric

50 reanalysis products. Temperature and humidity extremes from HadISDH by Willett (2023) are also designed for long-term regional trends. ~~The former has difficulty in evaluating long term trends because of sparsely distributed stations, with discontinuous and inhomogeneous observations (Dee et al., 2011),~~ The latter reanalysis dataset has issues of data quality that suffered from biases and errors from assimilated data during the satellite era, causing concerns about their reliability for detecting climate trends (Dai et al., 2011; Schröder et al., 2016; Trenberth et al., 2011). Trenberth et al. (2005) evaluated the

55 performance of global reanalyses, satellite, and radiosonde datasets on TPW and found that the Special Sensor Microwave Imager Sounder (SSM/I) dataset provided by Remote Sensing Systems (RSS) is the only source with reliable means, variabilities, and trends for TPW over oceans after 1988. The discontinuity and inaccurate data in 1992 due to changes in satellite instruments was highlighted by Trenberth et al (2015) and this spurious variability in water vapor existed in reanalyses up to the present ~~while in some of the previous reanalysis datasets, biases and errors in observations that are assimilated into~~

60 ~~the reanalyses system may affect the reanalysis dataset's quality and therefore cause concerns about their reliability for detecting climate trends (Dai et al., 2011; Schröder et al., 2016; Trenberth et al., 2011)~~. Numerous studies have analysed trends and variations in atmospheric water vapor distribution on both global and regional scales, primarily utilizing early versions of reanalysis datasets and satellite observations, albeit over relatively short study periods (e.g., Borger et al., 2022; Parracho et al., 2018; Wang et al., 2016; Zhang et al., 2019, 2021). New generation reanalysis datasets (JRA-55 and ERA5) provide a

65 better option for climate studies because of advanced modelling and data assimilation systems, with better accuracy, and fewer homogeneity issues (Hersbach et al., 2020; Kobayashi et al., 2015; Douville et al., 2022). JRA-55 showed a better performance in studying multidecadal variability and climate change than previous reanalysis datasets (Kobayashi et al., 2015). ~~and is reliable even for the pre-satellite era (Kikuchi, 2020).~~ Many studies have confirmed that ERA5 was the best or among the highest-performing reanalysis products (Taszarek et al., 2021; Yuan et al., 2023) although inhomogeneity still remains; for

70 example, water vapor associated with changes in SSMI instruments (Trenberth et al., 2015) and unreliability of tropical water vapor in ERA5 and ground-based observations before 1993 (Allan et al., 2022). Therefore, the latest ERA5 and JRA-55 were selected in this study to analyze long-term TPW changes and their relationship with temperatures at regional and global scales.

The near-surface air temperature (2m air temperature, T_{2m}) describes the thermodynamic temperature at a 1.5-2 m height while

75 surface skin temperature (T_s) refers to 'radiometric surface temperature' that is governed by the terrestrial radiation balance (Jin et al., 1997; Jin and Dickinson, 2010). Recent studies investigated how the TPW responds to changes in surface temperature using modelling estimation, satellite observations, or ground-based observation systems (Allan et al., 2022; Alshawaf et al., 2017; Borger et al., 2022; O'Gorman and Muller, 2010; Wang et al., 2016; Yuan et al., 2021), and many global surface temperature observational datasets use sea surface temperature (SST) over ocean and T_{2m} over land (e.g., HadCRUT,

80 Morice et al., 2021). Different from prior studies, we use the newest and longest available ~~reanalyses~~ reanalysis datasets to discuss the difference of T_{2m} and T_s, and ~~analyze~~ the relationship between trends in TPW and ~~surface temperature (T_{2m} and T_s)~~ from 1993 to 2021 ~~over the past 64 years, discuss the difference of T_{2m} and T_s~~ along with additional analysis using radiosonde data as well as AIRS and SSMI(S) satellite measurements since 2003. ~~and the potential discontinuities at global scale, and compare results with satellite and radiosonde data.~~

85
In this study, we focus on answering the following questions: (1) To what extent has the TPW changed ~~from 1958 to 2021~~ and what is the difference between the variations of T_{2m} and T_s on a multi-decade scale? (2) What is the relationship between trends of TPW changes and temperature changes? ~~Specifically, we analysis the trends in TPW and two temperatures (i.e, T_{2m} and T_s), as well as their relationships. W~~The results from reanalysis dataset are compared with radiosonde data as well as AIRS and

90 SSMI(S) satellite measurements ~~e then examine with satellite and radiosonde data.~~ ~~Lastly, we~~We discuss the difference of results among datasets and their potential discontinuities in datasets. Therefore, this paper is organized as follows. In section 2, we introduce the datasets and methods. In section 3, the TPW variations and the differences of T_{2m} and T_s are compared with radiosonde and satellite observations over land and ocean. Sections 4 and 5 provide the discussion and conclusion.

2 Data and Methods

2.1 Datasets

Two reanalysis datasets containing TPW and temperature (T_{2m}, T_s) from 1958 to 2021 were used in this study, these being ERA5 (Hersbach et al., 2020) and JRA-55 (Kobayashi et al., 2015). For ERA5, skin temperature, T_s, is the temperature estimated from the surface energy balance. For JRA-55, skin temperature is a diagnostic variable computed from the surface upward longwave radiation under the assumption that the surface is a black body. We used monthly reanalysis datasets from 100 January 1958 to December 2021 for TPW and temperatures. Both TPW and temperature variables in these two datasets were regirded into 1° x 1° resolution data using a bilinear interpolation method before analyzing (Zhuang, 2018).

The Atmospheric Infrared Sounder (AIRS) instrument captures a precisely calibrated, spectrally detailed dataset of both infrared and microwave radiances. It offers quality temperature and humidity profiles throughout the troposphere (Tian et al., 105 2020). Satellite observation from version 7 of AIRS (Tian et al., 2020) was used for comparison with the reanalysis from 2003 to 2021. The total column water vapor (kg m^{-2}) is calculated as the average of daytime (TotH2OVap_A) and nighttime modes (TotH2OVap_D). In addition, the column-integrated water vapor from the Special Sensor Microwave Imager and the Special Sensor Microwave Imager Sounder (SSMI(S)) from 2003-2021 (Wentz et al., 2015) are selected for comparison with reanalysis datasets.

110

We also used *in-situ* observations from the Radiosounding HARMonization (RHARM) dataset (Madonna et al., 2022), ~~which~~ which applied the new algorithm to the Global Climate Observing System Reference Upper-Air Network (GRUAN) data and used observation measurement instead of reanalysis data as a reference to calculate and adjust for systematic effects on temperature and humidity. ~~is a completely independent data source of reanalysis datasets.~~ RHARM provides homogenized 115 temperature and relative humidity profiles at two observation times (0000 and 1200 UTC) for radiosonde stations globally from 1979 to 2019. Therefore, T_{2m} used in this study from radiosonde observation was taken from the temperature observed at the lowest layer. Relative humidity and temperature from the surface to 500 hPa level are used to calculate precipitable water.

2.2 Methods

Monthly TPW and temperature anomalies were calculated by the base period of 1958-2021 for reanalysis datasets and 120 discussed the trends of long-term (1958-2021) and short-term (1993-2021) periods. We divided the globe into tropical regions (23.5°S–23.5°N), temperate (23.5°S–66.5°S in Southern Hemisphere (SH) and 23.5°N–66.5°N in Northern Hemisphere (NH)), and polar regions (66.5°S–90°S in SH and 66.5°N–90°N in NH). The regional average values, presented by different latitude bins, were calculated with a cosine (latitude) weighting factor to account for the convergence of grid points for each region. For the global distribution, all datasets were re-sampled into 1° x 1° resolution using spatial-averaging resampling, then 125 the area-weighted average of anomalies was computed to formulate a global time series.

For all trend analyses in TPW and temperature (T_s, T_{2m}) series, we selected the Seasonal Kendall (SK) test (Hirsch et al., 1982) using the Theil-Sen slopes (Sen 1968; Theil, 1992) to calculate relative TPW trends (% dec^{-1}) (Zhai and Eskridge, 1997) and temperature trends for both T_s and T_{2m} (K dec^{-1}). The statistical significance of all linear correlations and trends used was

130   performed at a 95% confidence level for all analyses conducted in this study. The TPW responses to temperature from 1993 to 2021 is calculated as ~~To obtain the percent change of TPW with respect to temperature, first the long-term trend of TPW (% dec^{-1}) and temperature trends (K dec^{-1}) are calculated, then~~ the ratio of TWP trends and ~~temperature~~ T_{2m} trends. ~~is calculated for the TPW responses to temperature.~~

135   Due to daily data missing in radiosonde observations, valid data required at least 10 days of data available within a month, and at least two-thirds of the total months had to have valid monthly data (345 months for 1979-2019). Each month had to have at least 28 years of valid data at each station to calculate monthly climatology. Trend analysis is also from Sen's estimate of the slope (Sen 1968) for these observations. Thereby, a set of 331 radiosonde stations were selected in this study. To facilitate the comparison, interpolated reanalysis data from radiosonde stations were selected to compare with the observation data. We

140   calculated the trend difference between reanalyses and observations to assess how effectively each reanalysis product captures ~~long-term~~ changes in observed TPW over 1979-2019.

To detect potential discontinuity within temporal sequence of total water vapor and temperature in ~~observation~~ reanalysis dataset, we applied penalized maximal F test (PMF test, Wang et al., 2006, ~~2006~~2013; Wang, ~~2008~~2018) to detect temporal

145   discontinuity points on ~~averaged monthly anomaly~~each grid over ocean~~, land, NH polar, North America, and Tropical land regions~~ during 1958-2021. The discontinuities were documented if testing statistic's p-value was less than 0.~~05~~01 (Zhou et al., 2021). ~~The magnitudes of shifts at discontinuity points, also called step sizes, are calculated for each discontinuity point. Then, discontinuity point positions were compared with changes in observing measurement systems. We defined the temporal coincidence when the discontinuity point positions were within a 3-month window along with observing measurement systems.~~

150   ~~Lastly, after identifications of discontinuity point's magnitudes and positions, the times series were adjusted using the quantile matching (QM) procedure (Wang et al., 2010). Trend comparisons were conducted before and after QM adjusted, and the RHtestsV4 tool is used for these calculations (Wang and Feng, 2013).~~

3 Results and Discussion

3.1 TPW Trends

155   ~~Figure 1 shows the decadal trends in TPW calculated from ERA5 and JRA-55 between 1958 and 2021. In general, the two reanalysis datasets showed similar trend patterns of global TPW distribution, with upward trends as the dominant change of TPW, indicating a rise in moisture in response to global warming since the twentieth century (Santer et al., 2006). TPW trends~~

are largely positive and statistically significant over North America, tropical land regions (± 23.5° band), and the NH polar region. On the other hand, decreasing TPW trends show a dipole structure over the Southern Ocean in both reanalysis datasets which can be attributed to the change of the ENSO phase (Trenberth et al., 2005). In contrast, these two reanalysis datasets show opposite trends over eastern Africa including the Sudan and Ethiopia where ERA5 trends are positive, whereas JRA-55 trends are negative. The reason for opposite trends in reanalyses is likely due to the different representations of large-scale moisture transport, surface-atmosphere processes, and their data assimilation (Parracho et al., 2018). Chen and Liu (2016) and Parracho et al. (2018) also showed decreasing trends in North Africa using ERA-Interim reanalysis for 1979-2014 and 1980-2016, and the biases in rainfall over West Africa might also exist in ERA-Interim reanalysis (Dunning et al., 2016).
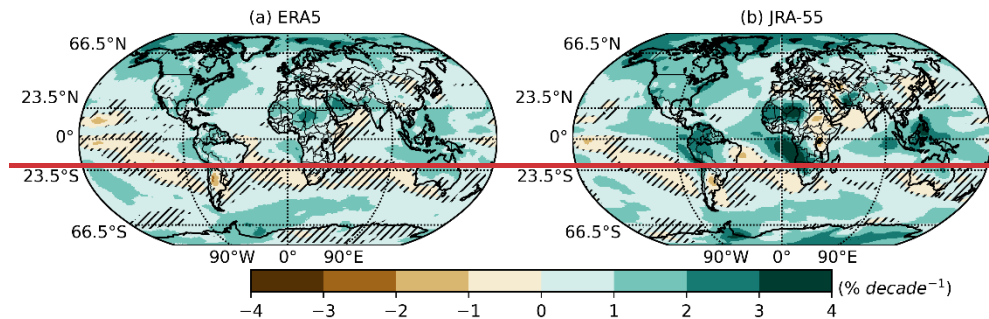

Figure 1. Monthly total precipitable water (TPW) trend (% dec⁻¹) from 1958 to 2021 from **(a)** ERA5 and **(b)** JRA-55. The hatch areas represent trends that are not statistically significant at a 95% confidence level.

Figures~~Figs~~. 2a~~1a~~-e show the temporal variations of monthly TPW anomalies over tropical, temperate, and polar regions. Overall, in terms of latitude bands, these trends differ little between the two reanalysis datasets. Specifically, ERA5 gives a 0.6~~1~~ % dec^{-1} moistening rate whereas the JRA-55 shows a 0.~~97~~96 % dec^{-1} moistening rate over the tropical regions for the whole period 1958-2021. A notable decrease in TPW is shown during the 1980s to 1990s over tropical regions in ERA5, which is consistent with ERA-interim (Allan et al., 2014) but inconsistent with satellite microwave data (Allan et al., 2022). This discrepancy seems to originate in the tropical lower troposphere over ocean~~during the 1980s to1990s over tropical regions in ERA5, which has been noted before and is consistent with satellite microwave data (Allan et al., 2022)~~. Since SSM/I satellite became available and were used in ERA5 after 1987 (Hersbach et. al., 2020), there has been some spurious variability in TPW, notably in January 1992 (Trenberth et al., 2015). However, a strong agreement of TPW after 1993 is shown between SSM/I observations and ERA5 (Allan et al., 2022). In addition, data after 1993 show fewer change points based on PMF-test results on grid boxes over the ocean (Figure S2). Thus, the 1993-2021 time series of TPW benefiting from in-situ and satellite observations is expected to produce more reliable water vapor variability. ERA5 gives a 1.46 % dec^{-1} moistening rate whereas the JRA-55 shows a 1.43 % dec^{-1} moistening rate over the tropical regions from 1993 to 2021. Trends range from 1.64 to 3.89 ~~0.82 to 1.95~~ % dec^{-1} over temperate and polar regions in NH and are about 1.56 (0.89) ~~0.44~~ % dec^{-1} over temperate but are not significant over polar in SH for ERA5 (JRA-55) during 1993-2021. ~~and 0.84 % dec⁻¹ over polar regions in SH for both~~

185 ~~reanalysis datasets.~~ The TPW trends increase in the NH is larger than those in the SH although they showed strong month-to-month variabilities (coefficient of variation, CV, is 0.7 on average) in the NH, which are consistent with the global distribution (Fig. 1).

Figures ~~2f~~1f-h depict these trends of TPW estimated over the ocean, land, and the globe. It is noticeable that monthly TPW
190 anomalies showed a consistent and statistically significant increase, yielding a rate of 0.~~57~~58 (0.85), 0.~~98~~88 (1.07), and 0.~~66~~65 (0.89) % dec^{-1} for ERA5 (JRA-55) during 1958-2021 ~~and 0.84, 1.05, and 0.88 % dec^{-1} for JRA-55~~ over ocean, land, and the globe, respectively. However, those trends increase at a rate of 1.72 (1.21), 1.19 (2.22) and 2.12 (1.91) % dec^{-1} for ERA5 (JRA-55) after 1993. The monthly TPW anomalies showed a similar variability over ocean, land, and globally (CVs, around 0.4), and displayed significant interannual variations, which had been dominated by ENSO events (Trenberth et al., 2005; Wang et
195 al., 2016). The distinct turning points may be attributed to the intensity of ENSO events. For example, one of the most powerful ENSO events during the 1997/1998 El Niña led to a significant tropical TPW increase, attributable to the warming in the equatorial Pacific (Wagner et al. 2005). The 2015/2016 El Niño caused a moistening TPW trend over tropical regions (Garfinkel et al., 2018). The trend of TPW during 1988-2003 was likely associated with the decadal variation of Interdecadal Pacific Oscillation from a warm period (1977-1998) to a cold period (1999 to 2003) (Dong and Dai, 2015). The TPW trend
200 for recent period including 1997/98 event will likely be similar (Wang et al. 2016). In addition, Patel and Kuttippurath (2023) also shows a strong correlation (0.81) between Pacific Decadal Oscillation and TPW variability in the tropics.
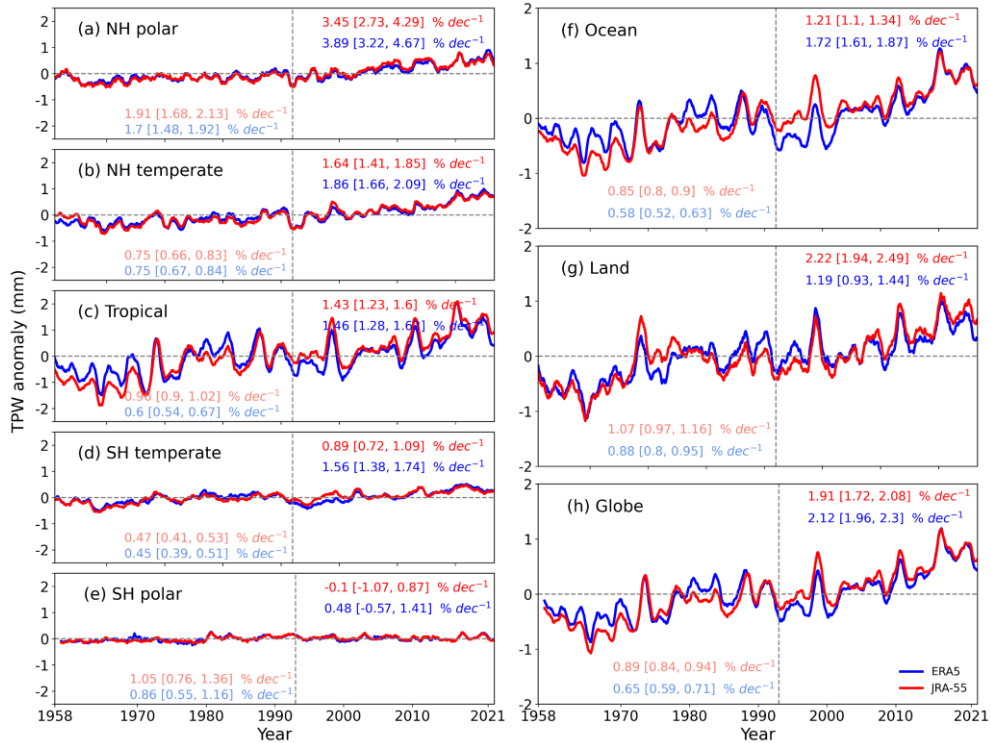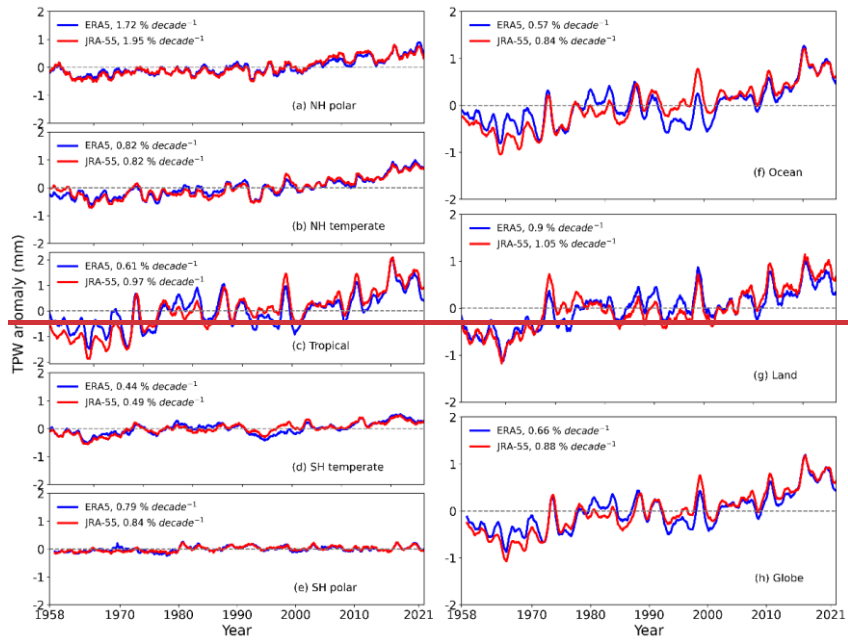
Figure 21. Time series of monthly TPW anomalies (mm) over **(a)** the Northern Hemisphere (NH) polar, **(b)** NH temperate, **(c)** Tropical, **(d)** Southern Hemisphere (**SH**) temperate, **(e)** SH polar, **(f)** ocean area, **(g)** land area, and **(h)** the globe from the ERA5 (blue curves) and JRA-55 (red curves) during the period 1958–2021. A 12-month running smoother was applied to each

time series shown. The trends are shown for 1958-2021 (light color) and 1993-2021 (dark color) periods with 95% confidence intervals in brackets. The vertical line indicates the year of 1993. All trends, shown in units of % per decade, were statistically

210 significant at a 95% confidence level.

Based on timeseries of TPW in Fig.1, Fig. 2 shows the decadal trends in TPW calculated from ERA5 and JRA-55 after 1993. In general, the two reanalysis datasets showed similar trend patterns of global TPW distribution, with upward trends as the dominant change of TPW, indicating a rise in moisture in response to global warming since the end of the twentieth century

215 (Santer et al., 2006). TPW trends are largely positive and statistically significant over North Africa, Europe and the NH polar region. In addition, Simpson et al. (2023) found that near-surface water vapor, as measured by surface observations, hasn't increased over arid and semi-arid regions since 1980, a discrepancy compared to predicted results from simulations. These findings indicate there might be misrepresentations of hydroclimate-related processes in simulations since climate models showed moistening trends associated with the increase in water vapor-holding capacity of a warmer atmosphere. On the other

220 hand, decreasing TPW trends show a dipole structure over the Southern Ocean in both reanalysis datasets which can be attributed to the change of the ENSO phase (Trenberth et al., 2005). In contrast, these two reanalysis datasets show opposite trends over eastern Africa including the Sudan where ERA5 trends are negative, whereas JRA-55 trends are positive. The reason for opposite trends in reanalyses is likely due to the different representations of large-scale moisture transport, surface-atmosphere processes, and their data assimilation (Parracho et al., 2018). Chen and Liu (2016) and Parracho et al. (2018) also

225 showed decreasing trends in North Africa using ERA-Interim reanalysis for 1979-2014 and 1980-2016, and the biases in rainfall over West Africa might also exist in ERA-Interim reanalysis (Dunning et al., 2016). In terms of TPW trend over arid and semi-arid regions from 1980 to 2020 in reanalysis dataset (figure not shown), it also shows a different trend, comparing observation from Simpson et al. 2023, that only TPW over southwest United States in ERA5 and central Africa in JRA-55 significantly decreased.
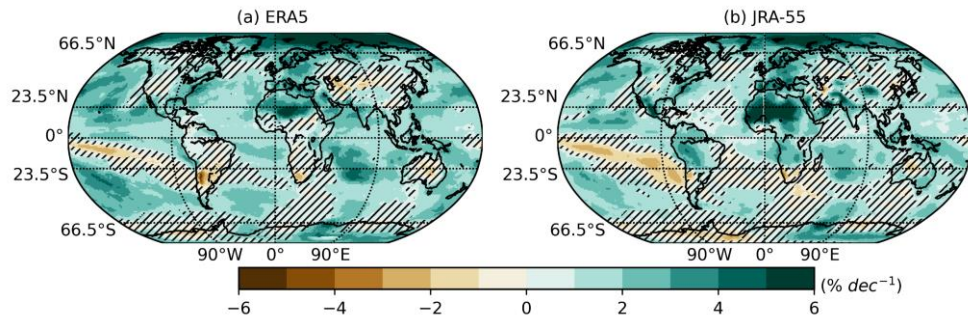

230

Figure 2. Monthly total precipitable water (TPW) trend (% dec^{-1}) from 1993 to 2021 from **(a)** ERA5 and **(b)** JRA-55. The hatch areas represent trends that are not statistically significant at a 95% confidence level.

9

3.2 Trends in temperature

235 In contrast to TPW, temperature in ERA5 is relatively stable for the pre-satellite era and aligned with independent datasets, although some notable discrepancies exist in accurately representing specific regional variations (Hersbach et al. 2020). The global trends of temperature ~~(T_{2m} and T_s)~~ between 1958-2021 exhibit widespread warming over large regions in both reanalysis datasets, except for some of small areas located in the SH and northern Atlantic (Fig. 3). Large land areas experience warming temperature changes of greater magnitude compared to the surrounding oceans (Fig. 3) and~~.~~ the ~~Both the trends of T_{2m} and T_s~~

240 ~~show a remarkably similar distribution, with a clear warming trend observed in the NH. The~~ strongest warming occurred in the Arctic (Fig. 3). Greater warming is observed over mid-latitude than tropical regions in NH, consistent with Zeng et al. (2021). Cooling in the North Atlantic is also observed by Li et al. (2022) when using observation datasets. This arises from strengthened local convection and heat dissipation from the ocean induced by the overlying atmosphere. Meanwhile, the North Atlantic cooling appears most significant in February in the northern hemisphere while it becomes net warming in August

245 (Allan and Allan, 2020). Some studies connect this phenomenon to changes in ocean circulation based on modeling results (Drijfhout et al., 2012). In addition, based on model simulations without considering variable ocean currents, He et al. (2022) explained that the warming hole is driven by enhanced surface westerly wind removing heat from ocean surface. For the SH, the polar region also experiences the strongest warming trends, similar to the trend's magnitudes by Clem et al. (2020). There is a slight difference between two reanalysis datasets for differential trends (ΔT) between T_s and T_{2m} at the global scale,

250 especially over the ocean area where ΔT trends are negative in ERA5 and positive in JRA-55. The ΔT shows a similar pattern only over the tropic land region (Fig. ~~3f~~3d). Although air and surface temperatures are closely related, they are physically distinct. The difference may be affected by changes of regional and seasonal vegetation ecosystems, land use, and land cover (Gulev et al., 2021; Masson-Delmotte, 2022). The ability of atmospheric reanalyses to effectively constrain variations in T_s and T_{2m} trends is limited because the sea surface temperatures in atmospheric reanalyses were obtained from globally observed

255 and interpolated products (Rayner et al. 2003). In contrast, the estimation of air temperature depends on model parameterizations and assimilated observations, which do not incorporate marine air temperature (Simmons et al., 2017). The strong correlations between T_{2m} and T_s are further discussed in SI (Fig. S4 &S5). Overall, T_{2m} and T_s show very similar interannual variations and the trends aren't significantly different. Therefore, we only present T_{2m} variations and its relationship with water vapor.
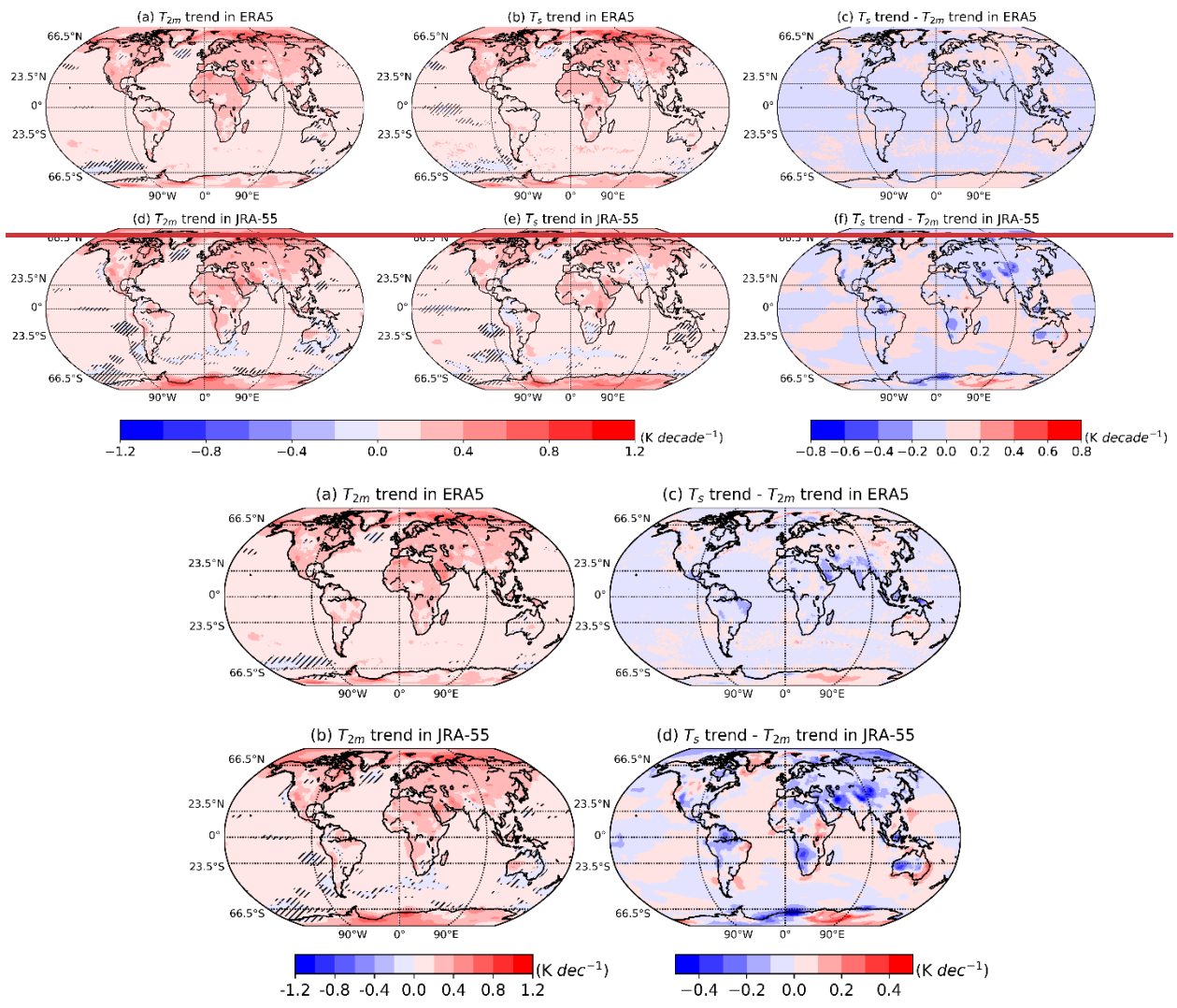
10

Figure 3. Trends of surface air temperature (T_{2m}) ~~(first column) and surface skin temperature (T_s) (second column)~~ from 1958 to 2021 for ERA5 (**a, ~~d~~**) and JRA-55 (**b, ~~e~~**). The differential trends between T_s and T_{2m} trends for ERA5 (**c**) and JRA-55 (**<ins>fd</ins>**). The hatch areas indicate trends that are not statistically significant. Trend units: K dec^{-1}.

<ins>The general warming since the late 1970s revealed by T_{2m}</ins> ~~Temperature trends (for T_s and T_{2m})~~ over different latitude bins in both datasets agree with each other when viewing the spatial distribution of magnitudes globally (Fig. 4), manifested by much larger warming in the Arctic at a rate (all temperature rates given as K dec^{-1}) of ~0.~~55~~<ins>45</ins>, which is ~~more than~~ three times warming than the global average rate (~0.15) (Figs. ~~4m~~<ins>4h</ins>, ~~4p~~). During the 1979-2021 period, this Arctic amplification of warming was markedly pronounced, occurring at rates 3.5 times faster than the global average warming rate documented by surface climate observations (Rantanen et al., 2022) in ERA5 data and 4 times faster in JRA-55 data. The potential causes of

11

the Arctic amplification may be linked to sea ice decline, changes in atmospheric and oceanic heat contents, or changes in atmospheric moisture transport (Graversen, 2006; Screen and Simmonds, 2010; Zhang et al., 2008). The Arctic warming is concentrated in the lower troposphere (Allan et al. 2022) and reached ~0.74 K dec^{-1} after 1993, thus leading to increases in

275   water vapor as shown in Fig. 1a. Antarctic warming is at a rate of ~0.2~4 K dec^{-1} over the past 64 years and consistent warming at ~0.23 K dec^{-1} after 1993. In addition, the warmer and colder years are linked to the ENSO events and further cause the distinct turning points of TPW (Fig. 1). but it should be noted that this warming rate is greater than 0.6 after 1980, which is consistent with surface observations (Rantanen et al., 2022). The datasets exhibit a clear consensus regarding the increased temperature of both land and ocean areas over the years. The land experienced greater warming at a rate exceeding 0.2 for

280   both T$_s$ and T$_{2m}$ compared to the oceans' warming, leading to a land-to-ocean warming ratio ranging from 1.8 to 2.3 (Fig. 4). The explained reasons for the land-ocean contrast in warming rates is the influence of temperature and humidity on lapse rate, which results in a smaller reduction in lapse rate over land areas compared to the ocean, leading to a greater warming effect on land surfaces than on ocean surfaces (Joshi et al., 2008). Additionally, the restriction of moisture in the land boundary layer directly contributes to an intensified warming of land surfaces, which, in turn, raises the lapse rate over the land (Joshi et al.,

285   2008). Byrne & O'Gorman (2018) further extended Joshi's theory in a quantitative way. They investigated the contrast of land/ocean warming from surface observations and model simulations at the global scale and indicated that amplified land temperature increases were the consequence of reduced relative humidity over land.
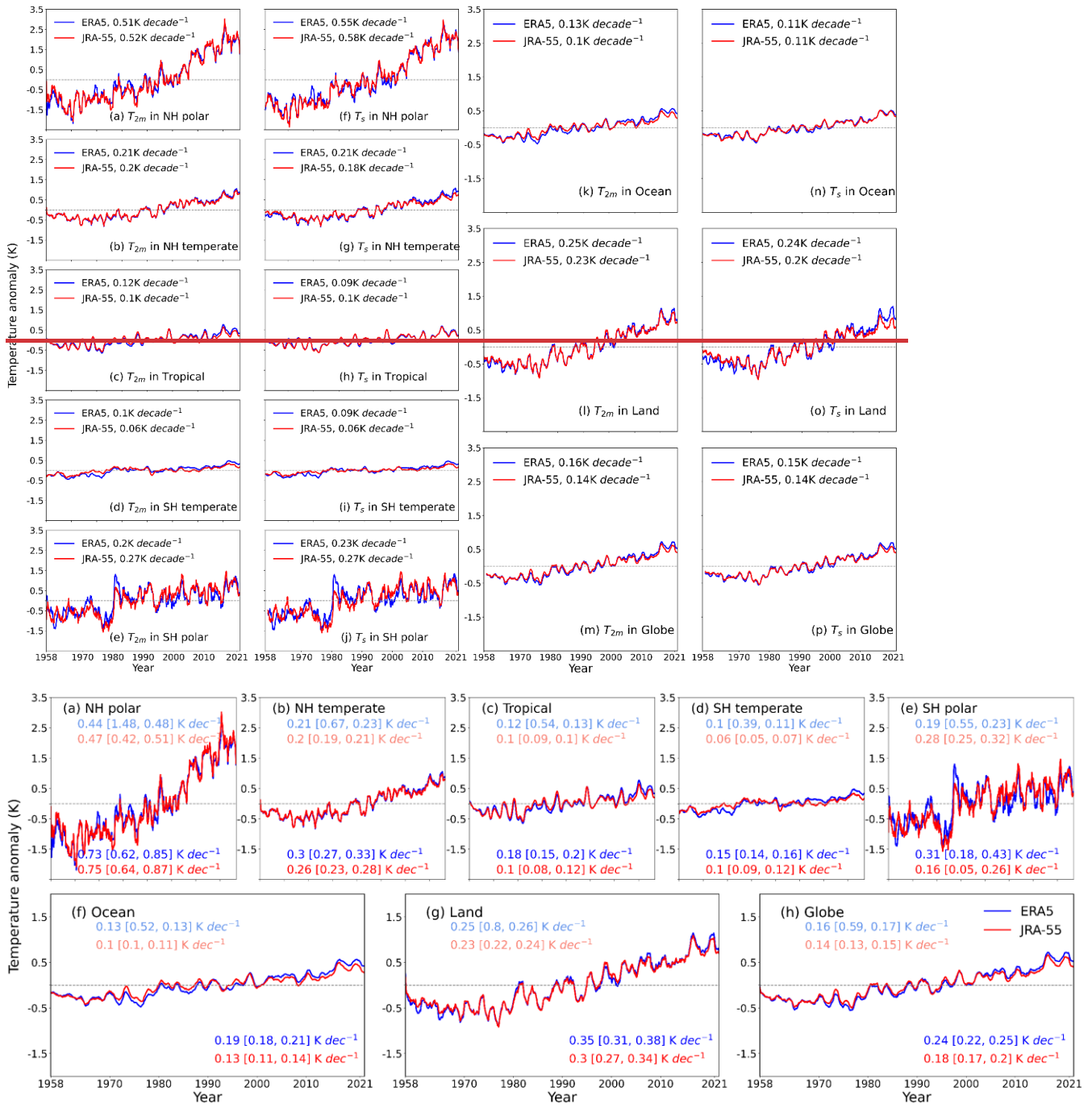
Figure 4. Monthly T$_{2m}$ and T$_s$ anomaly over (**a, f**) the Northern Hemisphere (**NH**) polar, (**b, g**) NH temperate, (**c, h**) Tropical, (**d, i**) Southern Hemisphere (**SH**) temperate, (**e, j**) SH polar, (**k, nf**) ocean, (**l, og**) land, and (**m, ph**) the globe from the ERA5 (blue ~~curves~~) and JRA-55 (red ~~curves~~) data sets during the period of 1958 to 2021. A 12-month running smoother was applied

13

to all time series. The trends are shown for 1958-2021 (light color) and 1993-2021 (dark color) periods with 95% confidence intervals in brackets. The vertical line indicates 1993 year. ~~All trends are statistically significant at a 95% confidence level.~~

3.3 TPW change response to temperature

TPW is expected to increase with air temperature by about 7% per K according to the Clausius–Clapeyron equation if the relative humidity in the lower troposphere is constant (Trenberth et al., 2005; O'Gorman and Muller, 2010). This relationship is determined by the ratio (dTPW/dT) of TPW trends and temperature trends from 1993 to 2021 (Fig. 5). The dTPW/dT ratio shows a similar pattern but different magnitude between two reanalysis datasets. The TPW increases significantly around 11.2% (10.9%), 5.8% (9.4%), and 9.5% (8.9%) per K for ocean, land, and globe for ERA5 (JRA-55). These rates are larger than 6% per K at a global scale based on observational HadCRUT5 (Allan et al., 2022). A disagreement involving TPW trend and tropospheric temperature trend between observation and modelling simulation is also shown in Santer et al. (2009, 2021)~~(Santer et al., 2021)~~. The dTPW/dT ratio increases significantly around 6% per K over eastern North America and Europe for both ERA5 and JRA-55 (Fig. 5). ~~The dTPW/dT ratio shows a similar pattern between T₂ₘ and Tₛ but there is a minor distinction between two reanalysis datasets. For ERA5, the TPW increases around 7.7%, 5%, and 6.5% per K for ocean, land, and globe, and close to 6% per K at a global scale based on observational HadCRUT5 (Allan et al., 2022), while these ratios are larger in JRA-55 (10.7%, 6.2%, and 8.6% per K, respectively). The dTPW/dT is generally around 6-8% per K over North America and NH polar regions for both ERA5 and JRA-55 (Fig. 5).~~ However, the relationship between TPW patterns and rising surface temperatures does not always follow the Clausius-Clapeyron equation, especially over some areas of Asia, central Africa, Australia and South American where TPW response to rising surface temperatures is negative without significance (Fig. 5). ~~However, TPW increase patterns with rising surface temperature do not always follow the Clausius-Clapeyron relation, especially over some areas of Asia and Europe where dTPW/dT ranges below 3 % per K and is even negative in central Africa (Fig. 5).~~ Regions with higher data density and homogeneity, such as North America and Europe, are likely to exhibit more realistic trends. Negative dTPW/dT occurs over the southern tropical ocean, where sea surface temperature was increased (Fig. 3) but precipitable water appears to be decreased slightly (Fig. 1); thus, the TPW change is contrary to what might be expected from the thermodynamic response to changes in temperature. Water vapor moves from one location to another through circulation, and the trend of vertical motion at 500 hPa could be further investigated to reveal the ascent and convective activity as well as its relationship to decreasing water vapor (Zveryaev and Allan, 2005).

14
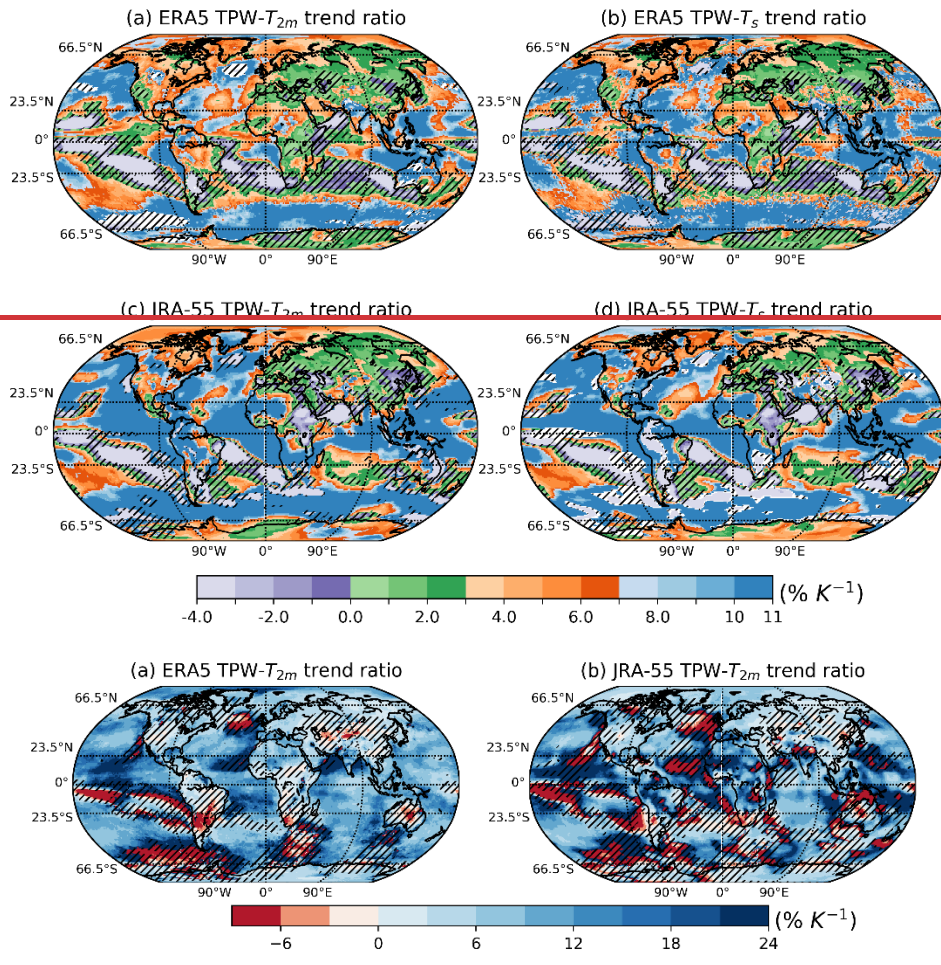
Figure 5. (a) The ratio (% K^{-1}) of the TPW trends and the surface air temperature (T$_{2m}$) trends from ~~1958~~ 1993 to 2021 in ERA5. **(b)** Same as **(a)** but for ~~surface skin temperature (T$_s$)~~JRA-55.~~. **(c)** Same as **(a)** but in JRA-55. **(d)** Same as **(a)** but for T$_s$ in JRA-55.~~The hatch areas represent ratios that are not statistically significant at the 95% confidence level.

In addition to the global patterns of spatial dTPW/dT ratios, the ratio's latitude dependency is an interesting subject (Fig. 6) between ~~60°~~55°S and ~~60°~~55°N. Although the TPW response values show strong variations across latitudes, the ratios show a similar changing pattern over the globe and ocean, which varies across the theoretical Clausius-Clapeyron curves of dTPW/dT ratios (Figs. 6a~~, c, d, f~~). The dTPW/dT ratios are close to the Clausius-Clapeyron response curves in NH mid- to high-latitudes over the ocean, but larger than 6% per K in the SH (-40 to -20°N band) over the ocean~~Over most of the NH, both dTPW/dT ratios are smaller than the Clausius-Clapeyron response curves, but they are close to the Clausium-Clapeyron relationship over temperate latitudes (-40 to -20°N band) in the SH for both the globe and ocean scales~~. Such strong latitude dependency and the discrepancy between land and ocean areas are associated with zonal relative humidity changes and possible amplification

15

of surface warming over land relative to the ocean (O'Gorman and Muller, 2010) (Figs. 6c, f). In arid areas, due to a lack of water, warming doesn't result in increased water vapor; conversely, in monsoon regions, the dynamics of the atmosphere amplify moisture increases (Fasullo, 2011). Multiple other studies also confirm the "dry gets drier, and wet gets wetter"

340 paradigm over land (Xiong et al., 2022). Likewise, an analysis of the salinity index in Cheng et al. (2024) showed that salty areas are getting saltier and fresh areas are getting fresher; and that over the ocean wet areas are getting wetter and dry areas are getting drier. There are two stronger TPW response zones, located in the southern highmid-latitude and the tropics over the globe and ocean (Figs. 6a, c, d, f). This result is nearly the same when drawn from multiple models of climate simulations for both historical and projected climate scenarios (O'Gorman and Muller, 2010). For land areas, in addition to two stronger

345 response zones similar to the globe and ocean, a local maximum was found in the sub-tropical areas of the NH and SH (Fig. 6). The ratios for the land region are mainly lower than the theoretical ratio (around 7% per K) and these ratios are even negative in tropical SH mid-latitudes where is the arid and semi-arid regions. Comparing these ratios between reanalysesbased on T_s and T_{2m}, their discrepancies are greater over landocean, which probably contributes to their discrepancies over the globe (Fig. 6).
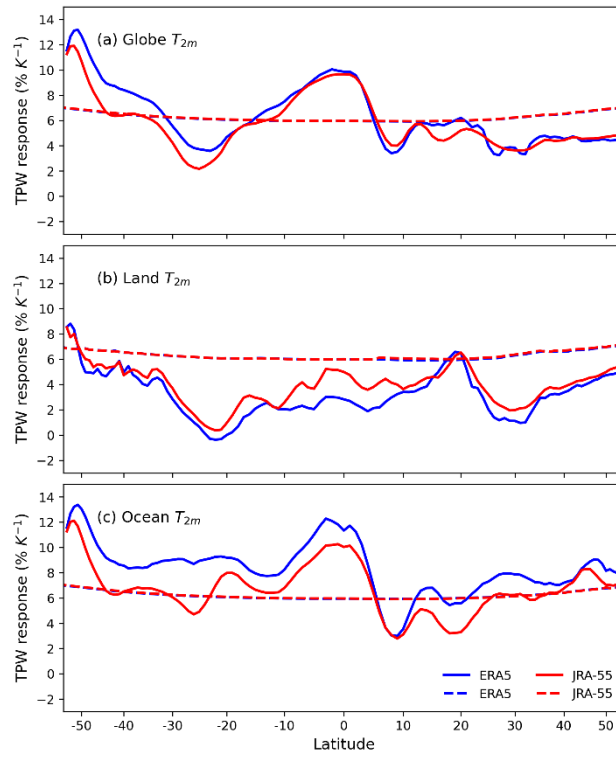
350
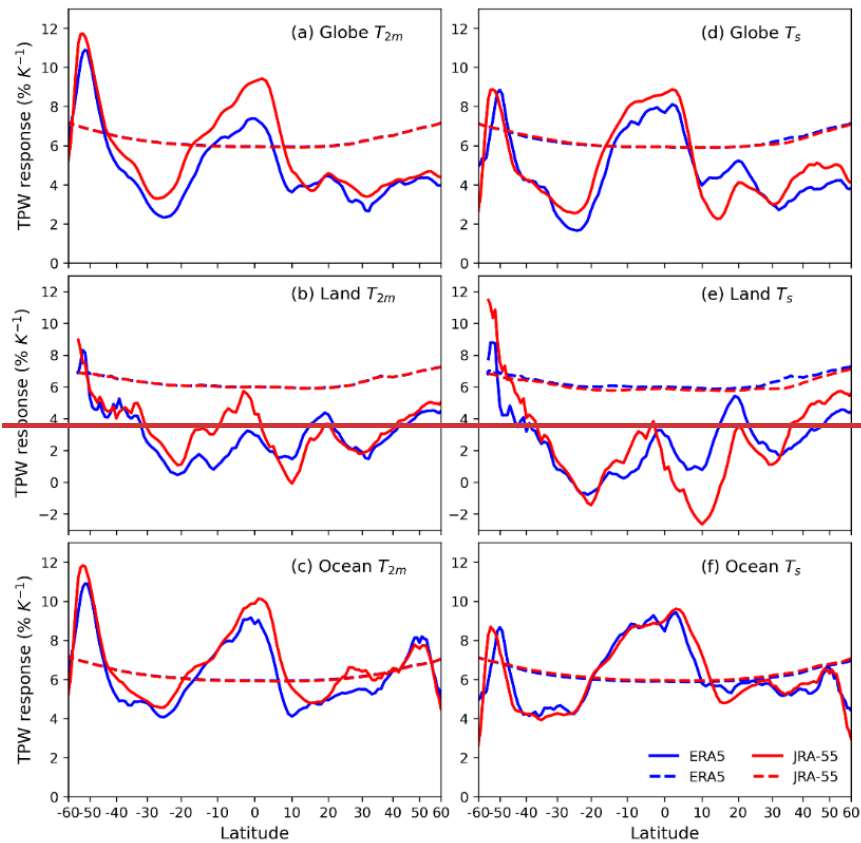
Figure. 6. The meridional means of change of TPW response to T_{2m} (first column) and T_s (second column) for ERA5 (blue lines) and JRA-55 (red lines) over **(a)** globe, **(b)** land, and **(c)** ocean base using data from 1993 to 2021. The dashed lines represent the theoretically expected Clausius-Clapeyron response based on the climatological zonal mean temperature from the trend analysis.

4 Further Discussion

The reanalysis dataset combines various observations to create a coherent global dataset using an atmospheric general circulation model. It provides spatially coherent and consistent data with global coverage, which makes it valuable for climate research (e.g., Allan et al., 2022; Urraca and Gobron, 2023). By assimilating multiple data sources and employing a physics-based model, reanalyses can effectively address uncertainties and minimize the presence of unrealistic values. However, it is worth mentioning that discontinuities in the time series may still occur in reanalysis datasets when satellites and conventional observations are transited, newly added, and removed during the assimilation process (Long et al., 2017). In order to get a general picture of discontinuities in the reanalysis data, we calculated the discontinuity from 1958 to 2021 for each grid box of temperature and TPW over the ocean, where there is a strong relationship between water vapor and temperature along with significantly increased trends (Figs. 1 and 3). We applied the PMF test on each grid of the reanalysis dataset and selected the significance level of 0.01 to detect discontinuities (Zhou et al., 2021). The years with detected discontinuities (after counting

17

all change points within the same year) of both temperature and TPW are shown in Figures S1 and S2. Discontinuities for temperature are relatively frequent before 1980 in both reanalysis datasets (Fig. S1a, b) and are relatively less frequent after 1980 for ERA5 except for 1992-1995, 1998, and 2015 when strong El Niño (1992, 1998, 2015) or La Niña (1995) events or a volcanic eruption (1992) occurred (Fig. S1c). It reveals that the detected change points during 1990-2021 in ERA5 might be associated with the result of abrupt climate changes. Previous studies also demonstrated the reliability of ERA5 air temperature for the warming trend of the global ocean (He et al., 2023; Wang et al., 2019). For TPW, discontinuities show a similar pattern as the temperature in ERA5, in which water vapor before 1980 has relatively more discontinuities. In addition, change points are fewer after 1980 except for the largest discontinuity in 1991-1992 (Fig. S2a) in ERA5 and in 1996-1997 in JRA-55 (Fig. S2b). Trenberth et al. (2015) highlighted that the discontinuity and inaccurate values in 1992 are the result of changes in satellite instruments. A strong agreement between SSMI(S) observations and ERA5 is shown after 1993 (Allan et al., 2022), and fewer discontinuities are presented from 1993 to 2021 (Fig. S2a). Meanwhile, discontinuities in JRA-55 are larger and distributed in all decadal periods even in normal years (Fig. S2b, c). Because TPW is highly dependent on temperatures and has a strong relationship with temperature over ocean, we further detected TPW discontinuities by comparing TPW and the expected TPW (TPW_{ept}) calculated from regression with temperature (Figure S3) during 1981-2021 when temperature shows fewer change points (Figure S1). The discrepancy points between TPW and TPW_{ept} are obvious over 1987, 1998, 1999, and 2015 in both analysis data, indicating the strong effect of ENSO events on the change of TPW. For ERA5, these discontinuities occurred in 1992 and 1995 when TPW_{ept} increased but TPW decreased in ERA5 (Fig. S2), in which the discontinuity in 1992 also existed in ERA-I (Trenberth et al., 2015). For JRA-55, discrepancy points occurred in 1984 and 1995. Due to lack of reliable observations before 1979, it is not recommended to use adjusted or statistically homogenized timeseries for trend analysis without metadata confirmation (e.g., the homogenized observations) (Wang and Feng, 2013). Although several discontinuities are detected in years after 1993 for TPW (Fig. S2), a strong agreement of TPW between ERA5 and SSMI satellite might indicate reliable TPW trends (Allan et al., 2022). Therefore, we used the PMF method to test potential discontinuities of the reanalysis dataset over ocean, land, NH polar, North America, and tropical land regions where both TPW and temperature trends increased significantly (Figs. 1 and 3). These potential discontinuity points are summarized (see Tables S1-3) (Hersbach et al., 2020; Kobayashi et al., 2015). Testing results indicate no significant discontinuities of TPW over the ocean in JRA-55, NH polar, and tropical land regions in ERA5 (see details in Table S1). The maximum magnitude of discontinuity in ERA5 occurred in January 1977 over the ocean region, coinciding with the change in the assimilation data from DMSP14 SSMI to DMSP 15 SSMI. In JRA-55, the maximum discontinuity's magnitude was in July 2003, which matches with the assimilation of AMSU and MHS satellite data in June 2003 (Kobayashi et al., 2015; Uppala et al., 2005). Most of discontinuities in TPW occurred after the satellite era (i.e., after 1979) when massive satellite data were introduced. It seems that 38% of the TPW discontinuities can be explained by changes that occurred in surface observing systems but 62% of discontinuities are not matched with changes in data sources or satellite changes during assimilation in reanalysis datasets (see Table S1). Due to these undocumented discontinuities, it is not recommended to use adjusted or statistically homogenized

18

timeseries for trend analysis without metadata confirmation (Wang and Feng, 2013) although there are slight differences between adjusted trends and raw trends (see Table S4).

For the surface temperatures, most of the discontinuities occur before the satellite era, therefore the long-term trend analysis for temperatures in reanalysis datasets after 1979 should be more reliable, and removing the effect of discontinuities located in the pre-satellite period on longer-term trends needs further investigation. In terms of temperature discontinuity identified (see Table S2 S3Figure S1), the longer temperature trends should be more reliable by using surface observation networks' datasets (Pielke et al., 2007). Overall, T₅ over the NH polar region in JRA-55, TPW over the ocean in JRA-55, as well as TPW over NH polar and tropical land regions in ERA5, are homogenous. Discontinuities are detected in other regions that may result in minimal alterations to the trends. This leads us to infer that, although the adjustments do enhance consistency during certain specific periods and reduce disparities concerning reanalysis data at the monthly and yearly scales, the adjusted data's trends in our study could often cause inconsistency due to undocumented discontinuities.

The RHARM radiosonde observations (Madonna et al., 2022), which are- mostly located in the NH land and available from 1979-2019, are completely independent of reanalysis data in terms of calculating and adjusting temperature and humidity. Compared with TPW trends from reanalysis data, moistening TPW in the NH polar region and Asia show the best agreement with radiosondes, with more than 90% and 60% of stations' trend differences within ± 0.2 mm dec^{-1}, respectively (Fig. S1S6). In addition, TPW trend differences are within ± 0.2 mm dec^{-1} at more than 54% of stations in Europe and North America (Fig. S1S6). Moistening TPW trends in Western Europe and South Asia and drying TPW trends in Western North America are consistent with the results from both reanalysis data and GPS observations (Parracho et al., 2018). Overall, ERA5 and JRA-55 show good agreement with observations at regional scales. Specifically, TPW shows better agreement in North America and the NH polar region.

After evaluating the reanalysis data with radiosonde observations on land, water vapor data from AIRS and SSMI(S) satellites are used to evaluate the accuracy of reanalysis over oceanic regions from 2003 to 2021 (Fig. S2S7). Except for the drying trends of the Northern Atlantic Ocean in the short-term period, the spatial drying trend patterns in the two reanalysis datasets are similar to the long-term trends (Fig.12) although they are not statistically significant. The surface air over tropical oceans increased in water vapor at a rate of 1.6 % dec^{-1} for ERA5 and 1.9 % dec^{-1} for JRA-55 on average, with a similar moistening rate shown in SSMI(S) (1.1% dec^{-1}) but not in AIRS data (0.05% dec^{-1}) since 2003. This result is consistent with Allan et al. (2022). The good agreement between the reanalyses and SSMI(S) is likely be attributed to the assimilation of all-sky radiances collected by the SSMI(S) satellite into the ERA5 and JRA-55 (Hersbach et al., 2020; Kobayashi et al., 2015). Although radiance measurement from AIRS is also introduced in ERA5 but not in JRA-55 (Hersbach et al., 2020; Kobayashi et al., 2015), the TPW from AIRS does not produce a strong global moistening and disagrees with reanalysis data and SSMI(S) microwave data and climate models, as well as Global Navigation System GPS (Allan et al., 2022; Douville et al., 2022).

5 Conclusions

Atmospheric reanalyses are widely used in the assessment of global climate change and their accuracy has advanced in recent years. Our study, bolstered by the latest ERA5 and JRA-55 reanalysis datasets, presents notable trends in the total precipitable water (TPW), surface temperature (T_s), and 2-meter temperature (T_{2m}) from ~~1958~~ 1993 to 2021. Beginning with TPW anomalies, a rise in moisture in response to global warming occurred from 1958-2021. However, due to data discontinuities in reanalysis data before 1993, more dependable trends have been identified. Post-1993, a moistening trend is observed at rates of 1.72% (ERA5) and 1.19% (JRA-55) per decade over oceans, 1.21% (ERA5) and 2.23% (JRA-55) per decade over land, and 2.12% (ERA5) and 1.90% (JRA-55) per decade globally. ~~based on large discontinuities in reanalysis during pre-1993 period, more reliable trends are shown with the increase at a rate of 1.72 (1.21), 1.19 (2.23) and 2.12 (1.9) % dec⁻¹ for ERA5 (JRA-55) after 1993 over ocean, land, and the globe.~~ When considering regional TPW trends, we identified statistically significant moistening trends over North ~~America~~Africa, Europe, ~~tropical land (±23.5° band),~~ and Northern Hemisphere polar regions since 1993. These findings, which are in concert with prior studies (Borger et al. 2022; Trenberth et al. 2005; Wang et al. 2016), point to the solitary exception of the South Pacific Ocean, where TPW trends registered as negative. The observed warming pattern is unlike coupled simulation, with warming more prominent in the tropical warm pool, which can increase stability in these subtropical subsidence regions (Andrews et al., 2022). Reanalysis ~~data~~ TPW showed an agreement with radiosonde observations over North America after 1979 and with SSMI(S) satellite but not AIRS measurement. ~~When considering TPW anomalies, we noted a consistent rise in both reanalysis datasets. Specifically, the moistening rates in ERA5 and JRA-55 were as follows: 0.57, 0.9, and 0.66 % per decade, and 0.84, 1.05, and 0.88 % per decade over ocean, land, and globe, respectively.~~

Building upon the analysis of TPW, our study further explored the temperature trends based on T_{2m} and T_s from ERA5 and JRA-55. Despite a general global warming trend (~ 0.15 K per decade), certain areas of the Southern Hemisphere and the North Atlantic Ocean demonstrated cooling since 1958. Terrestrial regions displayed a faster warming rate compared to oceanic regions, with a ratio of roughly 2:1, corroborating findings from Swaminathan et al. (2022). Arctic warming was particularly pronounced, registering three times the global average during 1958-2021, and escalating to around four times from 1979 to 2021 and around 6.5% K⁻¹ of water vapor response to temperature. While Antarctic warming was more modest at 0.2 K per decade over the past 64 years, a sharp increase to over 0.6 K per decade was observed post-1980.

Last, we examined the TPW response to surface temperature changes, noting deviations from the Clausius-Clapeyron relation. In the ERA5 dataset, we identified TPW increases of around ~~7.7~~11.2%, 5.~~8~~%, and ~~6~~9.5% per K for ocean, land, and globe, respectively after 1993. These increased rates were higher in the JRA-55 dataset, with values at 10.~~7~~9%, ~~6.2~~9.4%, and 8.~~6~~9%

20

per K, respectively. Importantly, these response ratios were not uniform globally, presenting a variation between 6 and 8% K^{-1} between latitudes 15 - ~~60°N~~ 55°N and increasing toward southern high latitudes over oceans. The most substantial ratios for deviations in TPW responses were discovered in the southern high latitudes across land, ocean, and the globe. Because of the importance of atmospheric water vapor in the global energy balance and hydrological cycle, it has received much attention in recent years (this study; Trent et al., 2023; Douville and Willett, 2022; Patel and Kuttippurath, 2023; Shao et al., 2023; Ding et al., 2022). In the near future, results from these studies need to be synthesized to further quantify atmospheric water vapor, its relationship with surface temperature, and associated uncertainties. These results can then be used to better evaluate climate models and constrain these models' future projections.

References

Allan, D. and Allan, R. P.: Seasonal Changes in the North Atlantic Cold Anomaly: The influence of cold surface waters from coastal greenland and warming trends associated with variations in subarctic sea ice cover, J. Geophys. Res. Oceans, 124, 9040–9052, https://doi.org/10.1029/2019JC015379, 2020.

Allan, R. P., Liu, C., Zahn, M., Lavers, D. A., Koukouvagias, E., and Bodas-Salcedo, A.: Physically consistent responses of the global atmospheric hydrological cycle in models and observations, Surv. Geophys., 35, 533–552, https://doi.org/10.1007/s10712-012-9213-z, 2014.

Allan, R. P., Willett, K. M., John, V. O., and Trent, T.: Global ~~Changes~~ changes in ~~Water~~ water ~~Vapor~~ vapor 1979–2020, J. Geophys. Res., 127, e2022JD036728, https://doi.org/10.1029/2022JD036728, 2022.

Alshawaf, F., Balidakis, K., Dick, G., Heise, S., and Wickert, J.: Estimating trends in atmospheric water vapor and temperature time series over Germany, Atmos. Meas. Tech., 10, 3117–3132, https://doi.org/10.5194/amt-10-3117-2017, 2017.

Andrews, T., Bodas-Salcedo, A., Gregory, J. M., Dong, Y., Armour, K. C., Paynter, D., Lin, P., Modak, A., Mauritsen, T., Cole, J. N. S., Medeiros, B., Benedict, J. J., Douville, H., Roehrig, R., Koshiro, T., Kawai, H., Ogura, T., Dufresne, J.-L., Allan, R. P., and Liu, C.: On the effect of historical SST patterns on radiative feedback, J. Geophys. Res. Atmos., 127, e2022JD036675, https://doi.org/10.1029/2022JD036675, 2022.

Bock, O. Global GNSS integrated water vapour data, 1994-2021 [Data set]. AERIS. https://en.aeris-data.fr/landing-page/?uuid=df7cf172-31fb-4d17-8f00-1a9293eb3b95

Borger, C., Beirle, S., and Wagner, T.: Analysis of global trends of total column water vapour from multiple years of OMI observations, Atmos. Chem. Phys., https://doi.org/10.5194/acp-2022-149, 2022.

Byrne, M. P. and O'Gorman, P. A.: Trends in continental temperature and humidity directly linked to ocean warming, Natl. Acad. Sci. U. S. A., 115, 4863–4868, https://doi.org/10.1073/pnas.1722312115, 2018.

Chen, B. and Liu, Z.: Global water vapor variability and trend from the latest 36 year (1979 to 2014) data of ECMWF and NCEP reanalyses, radiosonde, GPS, and microwave satellite, J. Geophys. Res., 121, 11,442-11,462, https://doi.org/10.1002/2016JD024917, 2016.

Clem, K. R., Fogt, R. L., Turner, J., Lintner, B. R., Marshall, G. J., Miller, J. R., and Renwick, J. A.: Record warming at the South Pole during the past three decades, Nat. Clim. Chang., 10, 762–770, https://doi.org/10.1038/s41558-020-0815-z, 2020.

Cheng, L., Abraham, J., Trenberth, K. E., Boyer, T., Mann, M. E., Zhu, J., Wang, F., Yu, F., Locarnini, R., Fasullo, J., Zheng, F., Li, Y., Zhang, B., Wan, L., Chen, X., Wang, D., Feng, L., Song, X., Liu, Y., Reseghetti, F., Simoncelli, S., Gouretski, V., Chen, G., Mishonov, A., Reagan, J., Von Schuckmann, K., Pan, Y., Tan, Z., Zhu, Y., Wei, W., Li, G., Ren, Q., Cao, L., and Lu, Y.: New record ocean temperatures and related climate indicators in 2023, Adv. Atmos. Sci., https://doi.org/10.1007/s00376-024-3378-5, 2024.

Dai, A., Wang, J., Thorne, P. W., Parker, D. E., Haimberger, L., and Wang, X. L.: A new approach to homogenize daily radiosonde humidity data, J. Clim., 24, 965–991, 2011.

Dee, D. P., Uppala, S. M., Simmons, A. J., Berrisford, P., Poli, P., Kobayashi, S., Andrae, U., Balmaseda, M. A., Balsamo, G., and Bauer, d P.: The ERA-Interim reanalysis: Configuration and performance of the data assimilation system, Q. J. R. Meteorol. Soc., 137, 553–597, 2011.

Ding, J., Chen, J., and Tang, W.: Increasing trend of precipitable water vapor in Antarctica and Greenland, in: China Satellite Navigation Conference (CSNC 2022) Proceedings, Singapore, 286–296, https://doi.org/10.1007/978-981-19-2588-7_27, 2022.

535   Dong, B. and Dai, A.: The influence of the Interdecadal Pacific Oscillation on temperature and precipitation over the globe, Clim Dyn, 45, 2667–2681, https://doi.org/10.1007/s00382-015-2500-x, 2015

Douville, H. and Willett, K. M.: A drier than expected future, supported by near-surface relative humidity observations, Sci. Adv., 9, eade6253, https://doi.org/10.1126/sciadv.ade6253, 2022.

Douville, H., Qasmi, S., Ribes, A., and Bock, O.: Global warming at near-constant tropospheric relative humidity is supported

540   by observations, Commun Earth Environ, 3, 1–7, https://doi.org/10.1038/s43247-022-00561-z, 2022.

Drijfhout, S., Oldenborgh, G. J. van, and Cimatoribus, A.: Is a decline of AMOC causing the warming hole above the North Atlantic in observed and modeled warming patterns?, J. Clim., 25, 8373–8379, https://doi.org/10.1175/JCLI-D-12-00490.1, 2012.

Dunning, C. M., Black, E. C. L., and Allan, R. P. The onset and cessation of seasonal rainfall over Africa. J. Geophys. Res.,

545   121(19), 11, 405-11, 424. https://doi.org/10.1002/2016JD025428, 2016.

Fasullo, J.: A mechanism for land–ocean contrasts in global monsoon trends in a warming climate, Clim. Dyn., 39, 1137–1147, https://doi.org/10.1007/s00382-011-1270-3, 2012.

Garfinkel, C. I., Gordon, A., Oman, L. D., Li, F., Davis, S., and Pawson, S.: Nonlinear response of tropical lower-stratospheric temperature and water vapor to ENSO, Atmos. Chem. Phys., 18, 4597–4615, https://doi.org/10.5194/acp-18-4597-2018, 2018.

550   Graversen, R. G.: Do changes in the midlatitude circulation have any impact on the Arctic surface air temperature trend?, J. Clim., 19, 5422–5438, 2006.

Gulev, S. K., Thorne, P. W., Ahn, J., Dentener, F. J., Domingues, C. M., Gerland, S., Gong, D., Kaufman, D. S., Nnamchi, H. C., Quaas, J., Rivera, J. A., Sathyendranath, S., Smith, S. L., Trewin, B., von Schuckmann, K., and Vose, R. S.: Changing state of the climate system, in: Climate Change 2021: The Physical Science Basis. Contribution of Working Group I to the

555   Sixth Assessment Report of the Intergovernmental Panel on Climate Change, edited by: Masson-Delmotte, V.; Zhai, P.; Pirani, A.; Connors, S.L.; Péan, C.; Berger, S.; Caud, N.; Chen, Y.; Goldfarb, L.; Gomis, M.I.; Huang, M.; Leitzell, K.; Lonnoy, E.; Matthews, J.B.R.; Maycock, T.K.; Waterfield, T.; Yelekçi, O.; Yu, R.; Zhou, B., Cambridge University Press, Cambridge, United Kingdom and New York, NY, USA, 287–422, https://doi.org/10.1017/9781009157896.004, 2021.

He, C., Clement, A. C., Cane, M. A., Murphy, L. N., Klavans, J. M., and Fenske, T. M.: A north atlantic warming hole without

560   ocean circulation, Geophys. Res. Lett., 49, e2022GL100420, https://doi.org/10.1029/2022GL100420, 2022.

He, M., Qin, J., Lu, N., and Yao, L.: Assessment of ERA5 near-surface air temperatures over global oceans by combining MODIS sea surface temperature products and in-situ observations, IEEE Journal of Selected Topics in Applied Earth Observations and Remote Sensing, 16, 8442–8455, https://doi.org/10.1109/JSTARS.2023.3312810, 2023

Held, I. M. and Soden, B. J.: Robust ~~Responses~~ responses of the ~~Hydrological~~ hydrological ~~Cycle~~ cycle to ~~Global~~ global

565   ~~Warming~~warming, J. Clim., 19, 5686–5699, https://doi.org/10.1175/JCLI3990.1, 2006.

Hersbach, H. and Dee, D.: ERA5 reanalysis is in production, ECMWF Newsletter, Vol. 147, Reading, United Kingdom, 2016.

Hersbach, H., Bell, B., Berrisford, P., Hirahara, S., Horányi, A., Muñoz-Sabater, J., Nicolas, J., Peubey, C., Radu, R., Schepers, D., Simmons, A., Soci, C., Abdalla, S., Abellan, X., Balsamo, G., Bechtold, P., Biavati, G., Bidlot, J., Bonavita, M., De Chiara, G., Dahlgren, P., Dee, D., Diamantakis, M., Dragani, R., Flemming, J., Forbes, R., Fuentes, M., Geer, A., Haimberger, L., Healy, S., Hogan, R. J., Hólm, E., Janisková, M., Keeley, S., Laloyaux, P., Lopez, P., Lupu, C., Radnoti, G., de Rosnay, P., Rozum, I., Vamborg, F., Villaume, S., and Thépaut, J.-N.: The ERA5 global reanalysis, Q. J. R. Meteorol. Soc., 146, 1999–2049, https://doi.org/10.1002/qj.3803, 2020.

Hirsch, R. M., Slack, J. R., and Smith, R. A.: Techniques of trend analysis for monthly water quality data, Water Resour. Res., 18, 107–121, 1982.

Masson-Delmotte, V., Zhai, P., Pörtner, H.O., Roberts, D., Skea, J. and Shukla, P.R., Global Warming of 1.5°C: IPCC Special Report on Impacts of Global Warming of 1.5°C above Pre-industrial Levels in Context of Strengthening Response to Climate Change, Sustainable Development, and Efforts to Eradicate Poverty, Cambridge University Press, ISBN 9781009157940, 2022.

Jin, M. and Dickinson, R. E.: Land surface skin temperature climatology: benefitting from the strengths of satellite observations, Environ. Res. Lett., 5, 044004, https://doi.org/10.1088/1748-9326/5/4/044004, 2010.

Jin, M., Dickinson, R. E., and Vogelmann, A. M.: A Comparison of CCM2–BATS Skin Temperature and Surfacesurface-Air air Temperaturetemperature with Satellitesatellite and Surfacesurface Observationsobservations, J. Clim., 10, 1505–1524, https://doi.org/10.1175/1520-0442(1997)010<1505:ACOCBS>2.0.CO;2, 1997.

Joshi, M. M., Gregory, J. M., Webb, M. J., Sexton, D. M. H., and Johns, T. C.: Mechanisms for the land/sea warming contrast exhibited by simulations of climate change, Clim. Dyn., 30, 455–465, https://doi.org/10.1007/s00382-007-0306-1, 2008.

Kikuchi, K.: Extension of the bimodal intraseasonal oscillation index using JRA-55 reanalysis, Clim. Dyn., 54, 919–933, https://doi.org/10.1007/s00382-019-05037-z, 2020.

Kobayashi, S., Ota, Y., Harada, Y., Ebita, A., Moriya, M., Onoda, H., Onogi, K., Kamahori, H., Kobayashi, C., Endo, H., Miyaoka, K., and Takahashi, K.: The JRA-55 Reanalysisreanalysis: General general Specifications specifications and Basic basic Characteristicscharacteristics, J. Meteorol. Soc. Japan, 93, 5–48, https://doi.org/10.2151/jmsj.2015-001, 2015.

Lacis, A. A., Schmidt, G. A., Rind, D., and Ruedy, R. A.: Atmospheric CO2: Principal control knob governing Earth's temperature, Science, 330, 356–359, 2010.

Li, L., Lozier, M. S., and Li, F. Century-long cooling trend in subpolar North Atlantic forced by atmosphere: an alternative explanation. Clim. Dyn., 58(9–10), 2249–2267. https://doi.org/10.1007/s00382-021-06003-4, 2022.

Long, C. S., Fujiwara, M., Davis, S., Mitchell, D. M., and Wright, C. J.: Climatology and interannual variability of dynamic variables in multiple reanalyses evaluated by the SPARC Reanalysis Intercomparison Project (S-RIP), Atmos. Chem. Phys., 17, 14593–14629, https://doi.org/10.5194/acp-17-14593-2017, 2017.

Madonna, F., Tramutola, E., Sy, S., Serva, F., Proto, M., Rosoldi, M., Gagliardi, S., Amato, F., Marra, F., Fassò, A., Gardiner, T., and Thorne, P. W.: The nNew Radiosounding HARMonization (RHARM) Data data Set set of Homogenized

600   homogenized ~~Radiosounding~~ radiosounding ~~Temperature~~temperature, ~~Humidity~~humidity, and ~~Wind~~ wind ~~Profiles~~profiles
       ~~With~~ with ~~Uncertainties~~uncertainties, J. Geophys. Res., 127, e2021JD035220, https://doi.org/10.1029/2021JD035220,
       2022.

       Masson-Delmotte, V., Zhai, P., Pörtner, H.O., Roberts, D., Skea, J. and Shukla, P.R., Global Warming of 1.5°C: IPCC Special
       Report on impacts of global warming of 1.5°C above pre-industrial levels in context of strengthening response to climate
605   change, Sustainable Development, and Efforts to Eradicate Poverty, Cambridge University Press, ISBN 9781009157940,
       2022.

       Morice, C. P., Kennedy, J. J., Rayner, N. A., Winn, J. P., Hogan, E., Killick, R. E., Dunn, R. J. H., Osborn, T. J., Jones, P. D.,
       and Simpson, I. R.: An ~~Updated~~ updated ~~Assessment~~ assessment of ~~Near~~near-~~Surface~~surface ~~Temperature~~ temperature
       ~~Change~~ change From 1850: The HadCRUT5 ~~Data~~ data ~~Set~~set, J. Geophys. Res., 126, e2019JD032361,
610   https://doi.org/10.1029/2019JD032361, 2021.

       O'Gorman, P. A. and Muller, C. J.: How closely do changes in surface and column water vapor follow Clausius–Clapeyron
       scaling in climate change simulations?, Environ. Res. Lett., 5, 025207, https://doi.org/10.1088/1748-9326/5/2/025207,
       2010.

       Parracho, A. C., Bock, O., and Bastin, S.: Global IWV trends and variability in atmospheric reanalyses and GPS observations,
615   Atmos. Chem. Phys., 18, 16213–16237, https://doi.org/10.5194/acp-18-16213-2018, 2018.

       Patel, V. K. and Kuttippurath, J.: Increase in iropospheric water vapor amplifies global warming and climate change, Ocean-
       Land-Atmosphere Research, 2, 0015, https://doi.org/10.34133/olar.0015, 2023.

       Pielke, R., Nielsen-Gammon, J., Davey, C., Angel, J., Bliss, O., Doesken, N., Cai, M., Fall, S., Niyogi, D., Gallo, K. and Hale,
       R.: Documentation of uncertainties and biases associated with surface temperature measurement sites for climate change
620   assessment. Bull. Am. Meteorol., 88(6), 913–928. https://doi.org/10.1175/BAMS-88-6-913, 2007.

       Rantanen, M., Karpechko, A. Y., Lipponen, A., Nordling, K., Hyvärinen, O., Ruosteenoja, K., Vihma, T., and Laaksonen, A.:
       The Arctic has warmed nearly four times faster than the globe since 1979, Commun. Earth Environ., 3, 1–10,
       https://doi.org/10.1038/s43247-022-00498-3, 2022.

       Rayner, N. A., Parker, D. E., Horton, E. B., Folland, C. K., Alexander, L. V., Rowell, D. P., Kent, E. C., and Kaplan, A.:
625   Global analyses of sea surface temperature, sea ice, and night marine air temperature since the late nineteenth century, J.
       Geophys. Res., 108, https://doi.org/10.1029/2002JD002670, 2003.

       Ruckstuhl, C., Philipona, R., Morland, J., and Ohmura, A.: Observed relationship between surface specific humidity, integrated
       water vapor, and longwave downward radiation at different altitudes, J. Geophys. Res., 112, 2007.

       Santer, B. D., Wigley, T. M. L., Gleckler, P. J., Bonfils, C., Wehner, M. F., AchutaRao, K., Barnett, T.P., Boyle, J.S.,
630   Bruggemann, W., Fiorino, M. and Gillett, N.: Causes of ocean surface temperature changes in Atlantic and Pacific tropical
       cyclogenesis regions. Proc. Natl. Acad. Sci. U.S.A., 103(38). https://www.osti.gov/biblio/922814, 2006.

       Santer, B. D., Taylor, K. E., Gleckler, P. J., Bonfils, C., Barnett, T. P., Pierce, D. W., Wigley, T. M. L., Mears, C., Wentz, F.
       J., Brüggemann, W., Gillett, N. P., Klein, S. A., Solomon, S., Stott, P. A., and Wehner, M. F.: Incorporating model quality

information in climate change detection and attribution studies, Natl. Acad. Sci. U. S. A., 106, 14778–14783, https://doi.org/10.1073/pnas.0901736106, 2009.

Santer, B. D., Po-Chedley, S., Mears, C., Fyfe, J. C., Gillett, N., Fu, Q., Painter, J. F., Solomon, S., Steiner, A. K., Wentz, F. J., Zelinka, M. D., and Zou, C.-Z.: Using climate model simulations to constrain observations, J. Clim., 34, 6281–6301, https://doi.org/10.1175/JCLI-D-20-0768.1, 2021.

Schröder, M., Lockhoff, M., Forsythe, J. M., Cronk, H. Q., Haar, T. H. V., and Bennartz, R.: The GEWEX ~~Water~~ water ~~Vapor~~ vapor ~~Assessment~~ assessment: ~~Results~~ results from ~~Intercomparison~~ intercomparison, ~~Trend~~ trend, and ~~Homogeneity~~ homogeneity ~~Analysis~~ analysis of ~~Total~~ total ~~Column~~ column ~~Water~~ water ~~Vapor~~ vapor, J. Appl. Meteorol. Climatol., 55, 1633–1649, https://doi.org/10.1175/JAMC-D-15-0304.1, 2016.

Screen, J. A. and Simmonds, I.: The central role of diminishing sea ice in recent Arctic temperature amplification, Nature, 464, 1334–1337, 2010.

Sen, P. K.: Estimates of the regression coefficient based on Kendall's tau, J. Am. Stat. Assoc., 63, 1379–1389, 1968.

Shao, X., Ho, S.-P., Jing, X., Zhou, X., Chen, Y., Liu, T.-C., Zhang, B., and Dong, J.: Characterizing the tropospheric water vapor spatial variation and trend using 2007–2018 COSMIC radio occultation and ECMWF reanalysis data, Atmos. Chem. Phys., 23, 14187–14218, https://doi.org/10.5194/acp-23-14187-2023, 2023.

Simmons, A. J., Berrisford, P., Dee, D. P., Hersbach, H., Hirahara, S., and Thépaut, J. N.: A reassessment of temperature variations and trends from global reanalyses and monthly surface climatological datasets, Q. J. R. Meteorol. Soc., 143, 101–119, https://doi.org/10.1002/qj.2949, 2017.

Simpson, I. R., McKinnon, K. A., Kennedy, D., Lawrence, D. M., Lehner, F., and Seager, R.: Observed humidity trends in dry regions contradict climate models, Natl. Acad. Sci. U. S. A., 121, e2302480120, https://doi.org/10.1073/pnas.2302480120, 2023.

Swaminathan, R., Parker, R. J., Jones, C. G., Allan, R. P., Quaife, T., Kelley, D. I., Mora, L. de, and Walton, J.: The ~~Physical~~ physical ~~Climate~~ climate at ~~Global~~ global ~~Warming~~ warming ~~Thresholds~~ thresholds as ~~Seen~~ seen in the U.K. Earth System Model, J. Clim., 35, 29–48, https://doi.org/10.1175/JCLI-D-21-0234.1, 2022.

Taszarek, M., Pilguj, N., Allen, J. T., Gensini, V., Brooks, H. E., and Szuster, P.: Comparison of ~~Convective~~ convective ~~Parameters~~ parameters ~~Derived~~ derived from ERA5 and MERRA-2 with ~~Rawinsonde~~ rawinsonde ~~Data~~ data over Europe and North America, J. Clim., 34, 3211–3237, https://doi.org/10.1175/JCLI-D-20-0484.1, 2021.

Theil, H.: A rank-invariant method of linear and polynomial regression analysis, in: Henri Theil's contributions to economics and econometrics, Springer, 345–381, 1992.

Tian, B., Manning, E., Roman, J., Thrastarson, H., Fetzer, E., and Monarrez, R.: AIRS Version 7 ~~Level~~ level 3 ~~Product~~ product ~~User~~ user ~~Guide~~ guide, 34, 2020.

Trenberth, K. E.: Atmospheric moisture residence yimes and cycling: implications for rainfall rates and climate change, Clim. Change, 39, 667–694, https://doi.org/10.1023/A:1005319109110, 1998.

Trenberth, K. E., Dai, A., Rasmussen, R. M., and Parsons, D. B.: The changing character of precipitation, Bull. Am. Meterol. Soc., 84, 1205–1218, https://doi.org/10.1175/BAMS-84-9-1205, 2003.

Trenberth, K. E., Fasullo, J., and Smith, L.: Trends and variability in column-integrated atmospheric water vapor, Clim. Dyn.Clim. Dyn., 24, 741–758, https://doi.org/10.1007/s00382-005-0017-4, 2005.

Trenberth, K. E., Fasullo, J. T., and Mackaro, J.: Atmospheric moisture transports from ocean to land and global energy flows in reanalyses, J. Clim., 24, 4907–4924, 2011.

Trenberth, K. E., Zhang, Y., Fasullo, J. T., and Taguchi, S.: Climate variability and relationships between top-of-atmosphere radiation and temperatures on Earth, J. Geophys. Res. Atmos., 120, 3642–3659, https://doi.org/10.1002/2014JD022887, 2015.

Trent, T., Schroeder, M., Ho, S.-P., Beirle, S., Bennartz, R., Borbas, E., Borger, C., Brogniez, H., Calbet, X., Castelli, E., Compo, G. P., Ebisuzaki, W., Falk, U., Fell, F., Forsythe, J., Hersbach, H., Kachi, M., Kobayashi, S., Kursinsk, R. E., Loyola, D., Luo, Z., Nielsen, J. K., Papandrea, E., Picon, L., Preusker, R., Reale, A., Shi, L., Slivinski, L., Teixeira, J., Vonder Haar, T., and Wagner, T.: Evaluation of total column water vapour products from satellite observations and reanalyses within the GEWEX water vapor assessment, Climate and Earth System/Remote Sensing/Troposphere/Physics (physical properties and processes), https://doi.org/10.5194/egusphere-2023-2808, 2023.

Uppala, S. M., KÅllberg, P. W., Simmons, A. J., Andrae, U., Bechtold, V. D. C., Fiorino, M., Gibson J. K, Haseler J., Hernandez A., Kelly G. A., Li X.: The ERA 40 re analysis. Q. J. R. Meteorol. Soc., 131(612), 2961-3012. https://doi.org/10.1256/qj.04.176, 2005.

Urraca, R. and Gobron, N.: Temporal stability of long-term satellite and reanalysis products to monitor snow cover trends, The Cryosphere, 17, 1023–1052, https://doi.org/10.5194/tc-17-1023-2023, 2023.

Wagner, T., Beirle, S., Grzegorski, M., Sanghavi, S., and Platt, U.: El Niño induced anomalies in global data sets of total column precipitable water and cloud cover derived from GOME on ERS-2, J. Geophys. Res., 110, https://doi.org/10.1029/2005JD005972, 2005.

Wang, C., Graham, R. M., Wang, K., Gerland, S., and Granskog, M. A.: Comparison of ERA5 and ERA-Interim near-surface air temperature, snowfall and precipitation over Arctic sea ice: effects on sea ice thermodynamics and evolution, The Cryosphere, 13, 1661–1679, https://doi.org/10.5194/tc-13-1661-2019, 2019.

Wang, J., Dai, A., and Mears, C.: Global Water water Vapor vapor Trend trend from 1988 to 2011 and Its its Diurnal diurnal Asymmetry asymmetry Based based on GPS, Radiosonderadiosonde, and Microwave microwave Satellite satellite Measurementsmeasurements, J. Clim., 29, 5205–5222, https://doi.org/10.1175/JCLI-D-15-0485.1, 2016.

Wang, X. L.: Penalized maximal F test for detecting undocumented mean shift without trend change. J. Atmos. Ocean. Technol., 25(3), 368–384. https://doi.org/10.1175/2007JTECHA982.1, 2018.

Wang, X. L., Chen, H., Wu, Y., Feng, Y., and Pu, Q.: New techniques for the detection and adjustment of shifts in daily precipitation data series. J. Appl. Meteorol. Climatol., 49(12), 2416–2436. https://doi.org/10.1175/2010JAMC2376.1, 2010.

700　Wang, X. L., and Feng, Y.: RHtestsV4 ~~User~~ user ~~Manual~~manual. Climate Research Division, ASTD, STB, Environment Canada, [Software]. http://etccdi.pacificclimate.org/software.shtml, 2013.

Wang, X. L., Swail, V. R., and Zwiers, F. W. Climatology and changes of extratropical cyclone activity: Comparison of ERA-40 with NCEP–NCAR reanalysis for 1958–2001. J. Clim., 19(13), 3145–3166. https://doi.org/10.1175/JCLI3781.1, 2006.

Wentz, F. J., Hilburn, K. A., and Smith, D. K.: Remote sensing systems DMSP [SSM/I or SSMIS][Daily, 3-Day, Weekly,
705　Monthly] environmental suite on 0.25° grid, Version 7 [Dataset]. Remote Sensing Systems, Santa Rosa, CA. https://www.remss. com/missions/ssmi, 2015.

Willett, K. M.: HadISDH.extremes Part I: A gridded wet bulb temperature extremes index product for climate monitoring, Adv. Atmos. Sci., 40, 1952–1967, https://doi.org/10.1007/s00376-023-2347-8, 2023.

Xiong, J., Guo, S., Abhishek, Chen, J., and Yin, J.: Global evaluation of the "dry gets drier, and wet gets wetter" paradigm
710　from a terrestrial water storage change perspective, Hydrol. Earth Syst. Sci., 26, 6457–6476, https://doi.org/10.5194/hess-26-6457-2022, 2022.

Yuan, P., Hunegnaw, A., Alshawaf, F., Awange, J., Klos, A., Teferle, F. N., and Kutterer, H.: Feasibility of ERA5 integrated water vapor trends for climate change analysis in continental Europe: An evaluation with GPS (1994–2019) by considering statistical significance, Remote Sens. Environ., 260, 112416, https://doi.org/10.1016/j.rse.2021.112416, 2021.

715　Yuan, P., Van Malderen, R., Yin, X., Vogelmann, H., Jiang, W., Awange, J., Heck, B., and Kutterer, H.: Characterisations of Europe's integrated water vapour and assessments of atmospheric reanalyses using more than 2 decades of ground-based GPS, Atmos. Chem. Phys., 23, 3517–3541, https://doi.org/10.5194/acp-23-3517-2023, 2023.

Zeng, X., Reeves Eyre, J. J., Dixon, R. D., and Arevalo, J.: Quantifying the occurrence of record hot years through normalized warming trends, Geophys. Res. Lett., 48, e2020GL091626, 2021.

720　Zhuang, J. xESMF: universal regridder for geospatial data. GitHub. GitHub repository, [Software]. https://doi.org/10.5281/zenodo.1134366, 2018.

Zhang, W., Lou, Y., Cao, Y., Liang, H., Shi, C., Huang, J., Liu, W., Zhang, Y., and Fan, B.: Corrections of ~~Radiosonde~~radiosonde-~~Based~~ based ~~Precipitable~~precipitable ~~Water~~ water ~~Using~~using ~~Ground~~ground-~~Based~~ based GPS and ~~Applications~~applications on ~~Historical~~historical ~~Radiosonde~~radiosonde ~~Data~~data ~~Over~~over China, J. Geophys. Res.,
725　124, 3208–3222, https://doi.org/10.1029/2018JD029662, 2019.

Zhang, W., Wang, L., Yu, Y., Xu, G., Hu, X., Fu, Z., and Cui, C.: Global evaluation of the precipitable-water-vapor product from MERSI-II (Medium Resolution Spectral Imager) on board the Fengyun-3D satellite, Atmos. Meas. Tech., 14, 7821–7834, https://doi.org/10.5194/amt-14-7821-2021, 2021.

Zhai, P., and Eskridge, R. E.: Atmospheric water vapor over China. J. of Clim., 10 (10), 2643–2652.
730　https://doi.org/10.1175/1520-0442(1997)010<2643:AWVOC>2.0.CO;2, 1997.

Zhang, X., Sorteberg, A., Zhang, J., Gerdes, R., and Comiso, J. C.: Recent radical shifts of atmospheric circulations and rapid changes in Arctic climate system, Geophys. Res. Lett., 35(22), https://doi.org/10.1029/2008GL035607, 2008.

Zhou, C., Wang, J., Dai, A., and Thorne, P. W.: A new approach to homogenize global subdaily radiosonde temperature data from 1958 to 2018, J. Clim., 34, 1163–1183, https://doi.org/10.1175/JCLI-D-20-0352.1, 2021.

735   Zveryaev, I. I. and Allan, R. P.: Water vapor variability in the tropics and its links to dynamics and precipitation, J. Geophys. Res.: Atm., 110, https://doi.org/10.1029/2005JD006033, 2005.